Structural, Electronic, and Mechanical Properties of Single-Walled Halloysite Nanotube Models

ARTICLE *in* THE JOURNAL OF PHYSICAL CHEMISTRY C · JULY 2010

Impact Factor: 4.77 · DOI: 10.1021/jp100902e

4 AUTHORS:

Luciana Guimaraes
Federal University of São João del-Rei
18 PUBLICATIONS **286** CITATIONS
SEE PROFILE

Andrey Enyashin
Institute of Solid State Chemistry, Ekaterin…
164 PUBLICATIONS **1,878** CITATIONS
SEE PROFILE

Gotthard Seifert
Technische Universität Dresden
428 PUBLICATIONS **14,369** CITATIONS
SEE PROFILE

Hélio A Duarte
Federal University of Minas Gerais
108 PUBLICATIONS **1,893** CITATIONS
SEE PROFILE

Structural, Electronic, and Mechanical Properties of Single-Walled Halloysite Nanotube Models

Luciana Guimarães,[†,‡] Andrey N. Enyashin,[§,||] Gotthard Seifert,[§] and Hélio A. Duarte*[,†]

Department of Chemistry, ICEx, Universidade Federal de Minas Gerais, 31.270-901 Belo Horizonte, MG, Brazil, Department of Natural Science, Universidade Federal de São João Del Rei, 36301-160, São João Del Rei, MG, Brazil, Physical Chemistry, Technische Universität Dresden, D-01062 Dresden, Germany, and Institute of Solid State Chemistry, Ural Branch of the Russian Academy of Science, 620990 Ekaterinburg, Russian Federation

Received: January 30, 2010; Revised Manuscript Received: April 27, 2010

Halloysite is a clay mineral with stoichiometry $Al_2Si_2O_5(OH)_4 \cdot nH_2O$ that can grow into long tubules and is chemically similar to kaolinite. In this work we present a systematic study on the stability, electronic, and mechanical properties of *zigzag* and *armchair* single-walled halloysite nanotubes by means of the self-consistent charge density-functional tight-binding method (SCC-DFTB). The detailed analysis is focused on structural properties, strain energy, and band gap as a function of tube radii and Mulliken charge distribution. The strain energy of halloysite nanotubes does not have a monotonic character and the most stable structures should be observed in the region of radii above 24 Å, in agreement with experimental data. Analysis of the electronic density of states shows that all tubes are insulators. Our calculations predict that single-walled halloysite nanotubes have Young modulus in the same order of imogolite and inorganic nanotubes, but smaller than that of carbon nanotubes. Even though most of the properties are adequately described by simpler halloysite models, further studies on multiwalled and larger diameter tubes are in progress.

Introduction

In the past decade, inorganic nanotubes (NTs) such as MoS_2, boron nitride, and WS_2[1−3] have significantly attracted researchers attention, principally due to unusual physicochemical, electrical, mechanical, and other properties of materials with tubular structure. Other inorganic nanotubes, like the clay minerals imogolite and halloysite, are being rediscovered in the nanoscience area.[4,5] Naturally occurring curved inorganic crystals had been speculated by Linus Pauling in 1930[6] in the context of chrysotiles and their structures had been reported in the 1950s.[7−10]

Imogolite[11] and halloysite[9] are naturally occurring aluminosilicate minerals with a predominantly hollow structure and different Al:Si ratio, 2:1 and 1:1, respectively. Imogolite is composed of single-walled nanotubes with stoichiometry $Al_2O_3(HO)_3SiOH$, where Si−OH groups are anchored to the inner side of the tube and a gibbsite octahedral sheet forms the outer side (Figure 1a). In contrast, halloysite consists of a gibbsite octahedral sheet ($Al(OH)_3$), which is modified by siloxane groups at the outer surface (Figure 1b). Halloysite has a 1:1 Al:Si ratio and stoichiometry $Al_2Si_2O_5(OH)_4 \cdot nH_2O$). It can grow into long multiwalled tubules, which are similar to some extent, particularly, in morphology, to multiwalled carbon NTs.[12]

Layered halloysite occurs mainly in two different polymorphs, the hydrated form (with interlayer spacing of 10 Å) with the formula $Al_2Si_2O_5(OH)_4 \cdot 2H_2O$ and the anhydrous form (with interlayer spacing of 7 Å) with the same chemical composition as kaolinite, $Al_2Si_2O_5(OH)_4$. The intercalated water is weakly held and can be readily and irreversibly removed.[12] The size of dehydrated halloysite particles varies from 500 to 1000 nm in length and 15 to 100 nm in inner diameter, depending on the substrate.[4,13]

Even though much less studied than carbon nanotubes, halloysite nanotubes are attractive materials due to their availability and the vast range of applications,[4] both biological and nonbiological. As demonstrated by Price et al.,[14,15] halloysite is a viable nanocage for biologically active molecules due to the empty space inside the nanotube allowing the entrance of molecules with specific sizes. Moreover, a supramolecular adduct of DNA-wrapped halloysite nanotubes has been reported for the first time, which extends the analogy with multiwalled carbon nanotubes.[16,17] Halloysite has been used as a support for immobilization of catalyst molecules such as metallocomplexes[18−20] and for the controlled release of anticorrosion agents, herbicides, and fungicides.[14,21,22] It exhibits interesting features and offers potential application as an entrapment of hydrophilic and lipophilic active agents,[16] as an enzymatic nanoscale reactor,[23] and in the sustained release of drugs;[13,15,24,25] and it can be employed to improve mechanical performance of cements and polymers.[26]

Notwithstanding, very little is currently known about the structural and electronic properties of halloysite NTs and as a consequence of renewed interest, a better understanding of the properties is needed. In this paper we present a systematic theoretical investigation of structure and electronic properties of single-walled halloysite nanotube models by means of self-consistent charge density-functional based tight-binding calculations (SCC-DFTB). The mechanical properties have also been studied due to its importance for practical applications. This is the first theoretical investigation that provides important information about the chemical properties of the halloysite nanotubes.

* To whom correspondence should be addressed. E-mail: duarteh@ufmg.br. Phone: (+55) (31) 3409 5748. Fax: (+55) (31) 3409 5700.
[†] Universidade Federal de Minas Gerais.
[‡] Universidade Federal de São João Del Rei.
[§] Technische Universität Dresden.
[||] Ural Branch of the Russian Academy of Science.

10.1021/jp100902e
Published on Web 06/14/2010

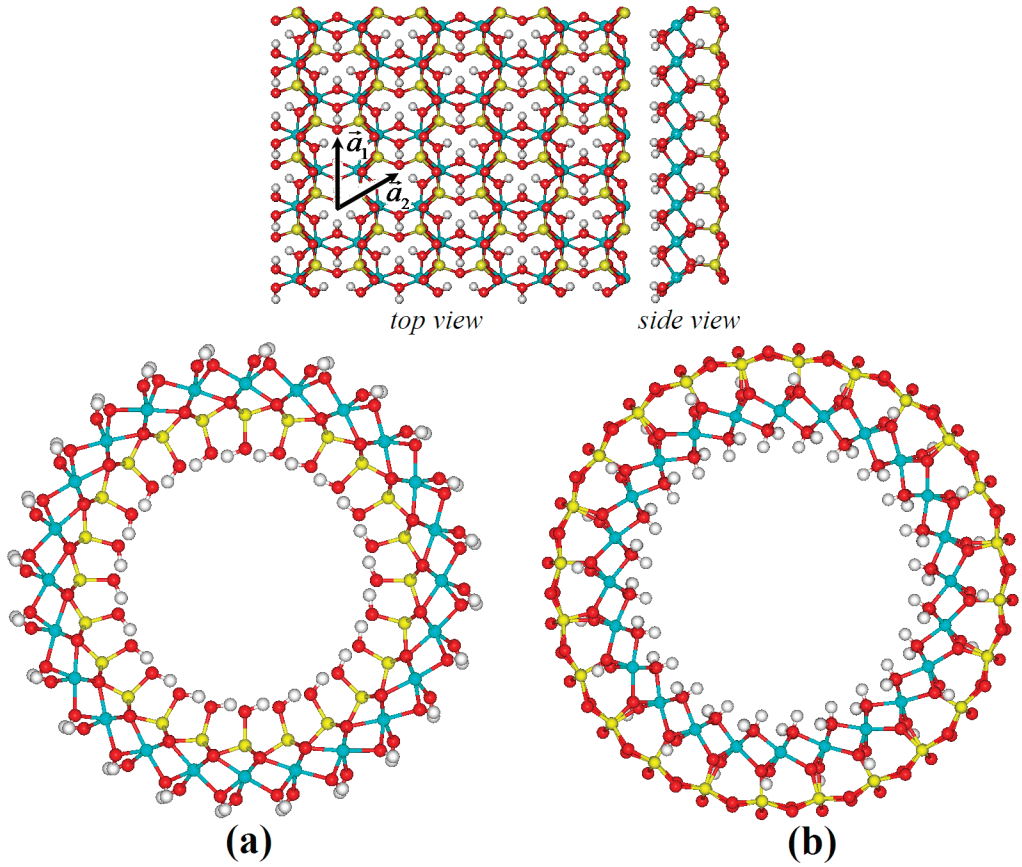

Figure 1. Structure of halloysite monolayer and cross section views of (a) a (12,0) imogolite nanotube and (b) a (12,0) halloysite nanotube. White atoms are H, red O, gray Al, and yellow Si.

Computational Details

All calculations have been carried out by using the self-consistent charge density-functional based tight-binding (SCC-DFTB)[27−29] method as implemented in DFTB+ code.[30] This method uses a minimal set of atomic basis functions and tight-binding like approximations to the Hamiltonian and can be applied for periodic and cluster computations. It has recently been shown that the DFTB method gives reliable results for structural, energetic, and electronic characteristics of imogolite,[31] $Al(OH)_3$,[32] and AlO(OH) nanotubes.[33]

Initial configurations of the nanotubes were constructed by folding the 2D halloysite layer (Figure 1). We adopt the same convention for labeling these tubes as was used for carbon, BN, and metal chalcogenides nanotubes. Depending on the rolling direction **B** in the 2D lattice $\mathbf{B} = n\mathbf{a_1} + m\mathbf{a_2}$ ($\mathbf{a_1}$, $\mathbf{a_2}$ are lattice vectors of the hexagonal lattice), three classes of nanotubes can be constructed: *armchair* (*n*,*n*), *zigzag* (*n*,0), and "chiral" (*n*,*m*) nanotubes with $n \neq m$. We have considered *zigzag* and *armchair* NTs with diameters ranging from 17 to 46 Å, which correspond to (8,0)...(20,0) and (5,5)...(15,15) configurations.

Initial structures have been fully optimized with respect to both atomic positions and tube cell length. The atoms are all independent of symmetry and the optimization process is performed without any constraint. Periodic boundary conditions were applied to the cells along tube axes. The Brillouin zone has been sampled by $1 \times 1 \times 6$ mesh points in *k* space.[34]

Results and Discussion

The optimized structures for *zigzag* (19,0) and *armchair* (11,11) single-walled nanotubes are shown in Figure 2 and the diameters of all tubes studied are listed in Table 1. The average Al−O, Si−O, and O−H bond lengths for optimized nanotube (19,0) are equal to 1.88, 1.68, and 0.96 Å. The bond distances differ by ±0.03 Å for other studied nanotubes and flat monolayer. The calculated bond distances are in agreement with the reported imogolite nanotubes (1.89 and 1.68 Å for Al−O and Si−O, respectively).[31] Although kaolinite is a planar sheet, we can also compare the calculated halloysite distances with kaolinite reported X-ray data (1.87 and 1.62 Å for Al−O and Si−O, respectively).[35]

It is important to call to the readers attention that the calculations have been performed for anhydrous form, and the results should carefully be considered before extrapolation to hydrous structure.

The calculated strain energy as a function of tube radius is depicted in Figure 3. The tube radius is based on the average distances of the oxygen atoms (siloxane groups) from the tube axis. The strain energy, E_{str}, is defined as the energy difference between the tube and an infinite layer, reflecting the energy required for the rolling of a planar sheet onto a cylinder. The thickness of a monolayer plays a crucial role in the stability of its nanotube. For nanotubes with the same radius but of different composition, an increase in the number of atomic planes within their walls results in larger E_{str} values. For instance, it grows in the series C→ MoS_2 → $Al(OH)_3$.[32] This result is not surprising once the rolling of a multiple layer into a tube causes more energy penalty than rolling a mono or double layer. Halloysite $Al_2Si_2O_5(OH)_4$ nanotubes with higher E_{str} values should have much larger radii than carbon nanotubes.

At first glance, the strain energy per atom for studied halloysite NTs (Figure 3) decreases with increasing tube radius (*R*) and converges approximately as $1/R^2$, i.e. as for other

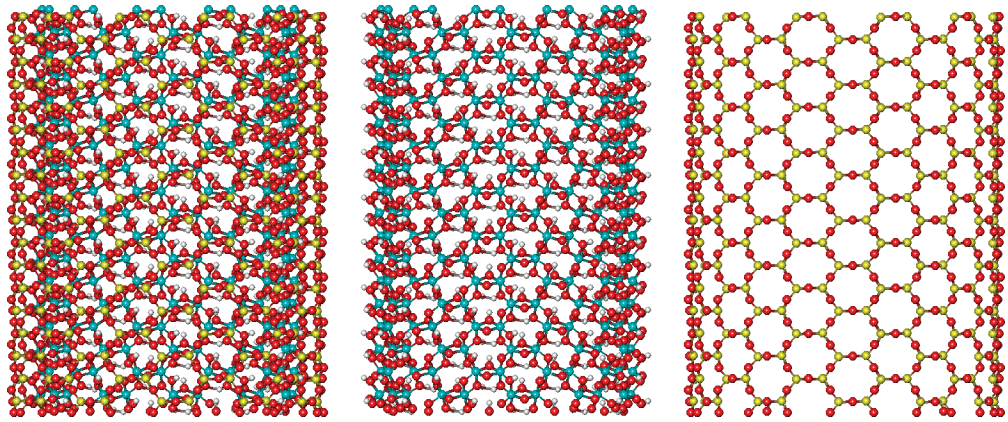

Figure 2. Optimized structure of an armchair (11,11) halloysite nanotube (side view on the left) and that decomposed on alumina and silica parts (in the middle and on the right, respectively). White atoms are H, red O, blue Al, and yellow Si.

TABLE 1: The Number of Atoms in the Unit Cell (*N*), Tube Diameter (*d*), Band Gaps (BG), and Young's Moduli (*Y*)

type	*N*	*d* (Å)	BG (eV)	*Y* (GPa)
		halloysite (*n,0*)		
(7,0)	238	15.65	2.7	234
(8,0)	272	17.28	3.6	246
(9,0)	306	18.91	4.2	308
(10,0)	340	20.44	4.9	298
(11,0)	374	21.99	5.6	285
(12,0)	408	23.51	6.2	286
(13,0)	442	25.04	6.7	288
(14,0)	476	26.60	7.1	280
(15,0)	510	28.20	7.4	275
(16,0)	544	29.80	7.7	273
(17,0)	578	31.43	7.9	264
(18,0)	612	33.06	8.1	274
(19,0)	646	34.69	8.3	277
(20,0)	680	36.33	8.4	280
		halloysite (*n,n*)		
(6,6)	204	21.10	5.1	308
(7,7)	238	23.84	6.3	322
(8,8)	272	26.51	7.3	327
(9,9)	306	29.23	7.9	305
(10,10)	340	32.12	8.5	339
(11,11)	374	34.79	8.9	319
(12,12)	408	37.64	9.1	306
(13,13)	442	40.47	9.2	302
(14,14)	476	43.36	9.3	302
(15,15)	510	46.19	9.4	301
infinite layer	34		9.9	

inorganic nanotubes such as MoS_2,[36] TiO_2,[37] and $Al(OH)_3$.[32] However, a detailed look at the calculated values E_{str} shows that they can be better fitted by the following equation (eq 1):

$$E_{str} = \frac{49.0}{R^2} - \frac{3.0}{R} \quad (1)$$

where R is the tube radius. For a wide region between 24 and 54 Å, halloysite nanotubes have slightly negative values for strain energies and are more stable than the respective monolayer. Thus, halloysite nanotubes are described by a similar equation used to fit the strain energies of imogolite nanotubes.[31] It is not an unexpected result, since halloysite nanotubes are composed of an asymmetrical aluminosilicate layer and should have different tension promoting the formation of a curved structure. For instance, if we plot the halloysite strain energies versus $1/R^2$ we find that points do not lie on a straight line (see Figure S1 in the Supporting Information).

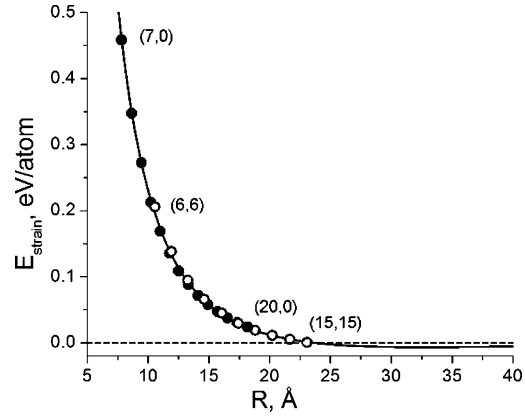

Figure 3. Strain energy as a function of tube radius for (*n*,0) (closed circles) and (*n*,*n*) (open circles) single wall nanotubes. Results are shown for (7,0)−(20,0) and (6,6)−(15,15) nanotubes.

Although the minimum of the E_{str} curve for halloysite nanotubes is much less pronounced when compared to that of imogolite nanotubes, the minimum is only 7 meV/atom below the energy of the layer, which is 5−6 times smaller than the corresponding values for imogolite (see Figure S2 in the Supporting Information). Calculations for larger nanotubes, which are in the intractable range with respect to our present computing resources, would be necessary to ensure the correct minimum. Nevertheless, eq 1 explains the morphological distinction between halloysite and imogolite experimental observations that exist as multiwalled and single-walled nanotubes, respectively. The strain energy difference between halloysite nanotubes is negligible enough explaining the existence of a set of multiwalled nanotubes with large radii distribution. In contrast, imogolite nanotubes are strongly monodisperse.

From Figure 3 one can also see that the strain energy of halloysite nanotubes is relatively insensitive to the detailed structures of tubes, as helicity.

Structural Properties. To support our structural model for halloysite nanotubes we have used their optimized unit cells within the DFTB method for X-ray diffraction simulations and the results have been compared with experimental data. The X-ray diffraction (XRD) techniques often have been applied by experimentalists to identify halloysite and to determine whether it is present in hydrated or dehydrated form. It has been recently shown that this method gives reliable results for

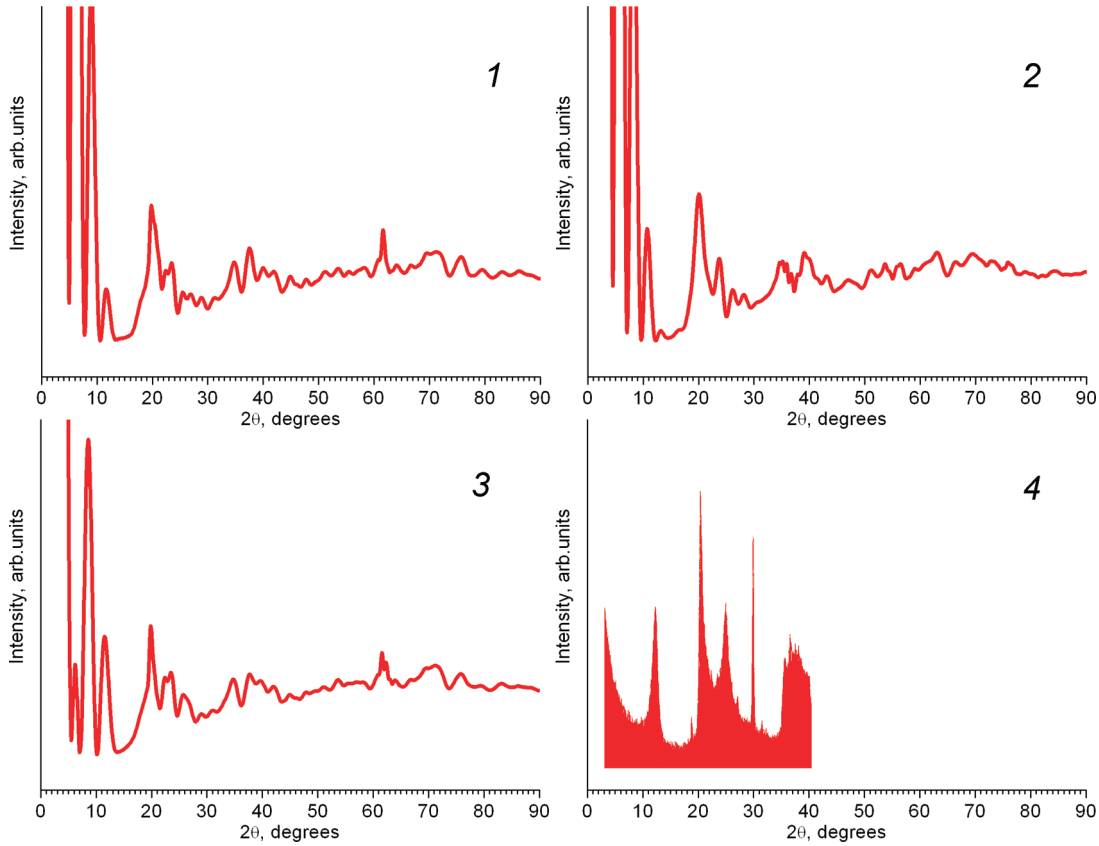

Figure 4. Experimental and simulated XRD spectra for halloysite nanotubes: (1) single-walled zigzag (19,0), (2) armchair (12,12), (3) double-walled (10,0)@(19,0), and (4) experimental data.[39]

imogolite nanotubes.[31] Our simulations were performed using the Debye formula (eq 2):

$$I(s) = \sum_i \sum_j f_i f_j \frac{\sin(sr_{ij})}{sr_{ij}} \qquad (2)$$

where r_{ij} is the distance between the ith and jth atoms, and f_i and f_j are the atomic scattering factors of the ith and jth atoms. s is the X-ray scattering vector and $s = 4\pi \sin(\theta/\lambda)$, with the diffraction angle 2θ, and the X-ray wavelength λ (in this work, 1.542 Å as for nickel filtered Cu Kα radiation). The values of the atomic scattering factors were taken from the International Tables for Crystallography.[38]

The theoretical XRD spectra for *zigzag* (19,0) and *armchair* (12,12) halloysite nanotubes are compared with the experimental data[39] in Figure 4. These tubes were selected since they have large diameters, approaching those of the experimentally studied tubes. The highlighted peaks in the experimental spectrum refer to dehydrated sample, which is characterized by a sharp peak in the region $2\theta = 12°$ corresponding to (001) reflection from the walls of coaxial multiwalled nanotubes. The analysis of results reveals a good correspondence between simulated and experimental spectra in the region of $20° < 2\theta < 40°$. In general, the XRD simulations support the structural model—atomic arrangement, bond lengths and angles—proposed for halloysite in this work. However, at small scattering angles there is not a pronounced similarity. The area 2θ below 15° for the case of single-walled nanotubes is composed of a fine system of numerous peaks of decaying intensity, which depends on the chirality of a tube. The peak near $2\theta = 12°$ has very small intensity or is absent. The intensity profile at this region is changed only considerably in the case of double-walled nanotubes (for example, (10,0)@(19,0) in Figure 4, panel 3). The intensity at $2\theta = 12°$ appears visible, while the structure and intensity of peaks below 12° become more ambiguous.

Using optimized unit cells for single-walled halloysite nanotubes we have analyzed also a few XRD patterns from double-walled halloysite nanotubes constructed from either the tubes of similar chirality (only *zigzag* or only *armchair*) or mixed chirality and having the interlayer distance of about 7 Å as in experimentally observed halloysite. However, we were not able to detect a complete similarity between theoretical and experimental XRD spectra as in our study of imogolite nanotubes.[14] This can be an additional proof for the absence of any favorite chirality among halloysite nanotubes: evidently, halloysite mineral is a mixture of multiwalled nanotubes of different chirality, which could be released also even within a single multiwalled tube.

Finally, we would like to note that, to the best of our knowledge, no satisfactory refinement on halloysite structure has been published. For example, Bates et al.[9] have assumed that the tetrahedral sheet is on the wall outer part. Mitra et al.[40] have stated that while it is extremely likely that the atomic layers in halloysite are curved, there is not a convincing model for its structure that can explain the experimentally observed X-ray diffraction pattern.

Electronic Properties. On the basis of optimized geometry, we have investigated the electronic properties of the halloysite planar layer and the corresponding tubular structures. The band gaps of *armchair* and *zigzag* nanotubes as a function of tube radius are presented in Figure S3 (Supporting Information). All nanotubes are insulators and the gap values for both chiralities increase with tube radii enlargement rising to the value of the planar layer (around 9.7 eV). Composite materials made by dispersing halloysite NTs

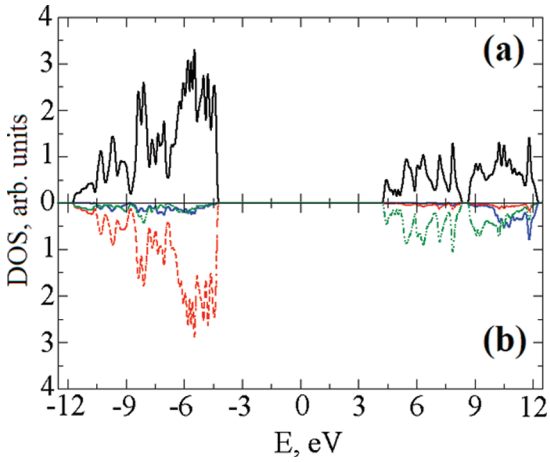

Figure 5. (a) Total and (b) partial density of states for (19,0) halloysite nanotube. (a) The black solid line is relative to total density of states; (b) the red line is relative to O atoms, the blue line is relative to Al atoms, and the green line is relative to Si atoms. All energies are given relative to Fermi level.

with insulating polymers do not change the insulating polymer properties and present good mechanical properties.[41,42] The total and partial density of states (DOS) for *zigzag* (19,0) halloysite NT is depicted in Figure 5, and the main features of the shown DOS graphic are similar to those of other sizes and chiralities. The valence band lower part (around −20 eV) is characterized by a contribution from oxygen 2s states while the higher energy part of the valence band (between −12 and −3 eV) is predominantly composed of oxygen 2p states. The oxygen atoms belonging to Al−O bonds have a predominant contribution to the valence band in comparison to the ones in Si−O bonds. The lower energy conduction band is mainly characterized by silicon and aluminum 3p and 3d states.

Halloysite is an aluminosilicate that has two different basal faces. The first one consist of a tetrahedral silicate surface Si−O−Si while the other basal surface has a gibbsite octahedral layer ($Al(OH)_3$). In principle, both faces are theoretically electrically neutral. The charges inside and outside halloysite nanotubes are related to their structure and adsorption properties. For this reason, the obtained optimized geometry and atomic Mulliken charges have been used to calculate the electrostatic potential map of some halloysite nanotubes, as shown in Figure 6. The results show that the inner wall of the tube is mainly positively charged, while the outer surface has a weakly negative charge. The Mulliken population analysis for optimized structures indicates the net charges on aluminum, silicon of about $Q \approx +0.4e$ and $+0.7e$), respectively. The oxygen atoms bound to aluminum and silicon have a net charge of $Q \approx -0.33e$ and $-0.4e$, respectively. These net charges are almost the same for all nanotubes, independent of the helicity and radius.

On the other hand, experimental results from natural samples indicate the halloysite structure at the edge is disrupted, and the surface groups can be protonated or deprotonated originating variable charge.[43] For instance, halloysite presents negative charge at pH higher than 3,[43] once its isoelectric point is around pH 3. In this way, the edges are considered to be positively charged at low pH, neutral at the isoeletric point, and negatively charged at higher pH.[44] The negative charge can be ascribed to the deprotonation of water and hydroxyl groups bound to aluminum and silicon at the edges,[43] and the hydroxyl groups are considered to be the principal reactive sites. Furthermore, Machado et al.[18] have shown that the immobilization of anionic and cationic metalloporphyrins into halloysite nanotubes occurs

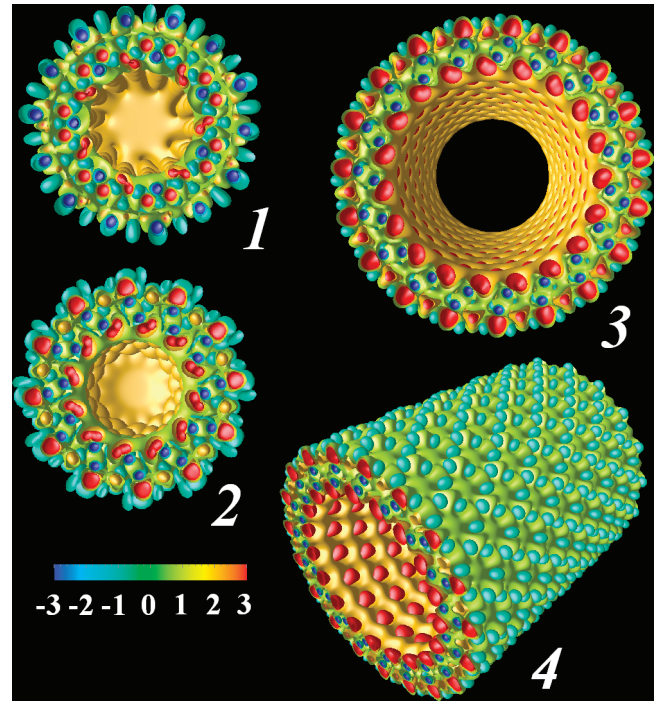

Figure 6. Electrostatic field nearby halloysite nanotubes of different chiralities: (1) armchair (7,7), (2) zigzag (12,0), (3) zigzag (19,0) (the views along the tubes' axis are shown), and (4) a diagonal view for zigzag (19,0) nanotube. Different colors show equipotential surfaces: −3.0, −2.0, −1.0, 1.0, 2.0, and 3.0 e/Å.

at high rates while for neutral metalloporphyrins the immobilization was not observed. The cationic immobilization can occur via SiO^- groups, while anionic immobilization may occur through aluminol groups at halloysite edges.

Mechanical Properties. The mechanical properties of halloysite are an important topic for applications of natural nanotubes. In the past few years,[26,42,45−47] halloysite NTs have been used as reinforcing material on polymers, increasing the modulus of polymer composite and improving its mechanical properties. Usually, experimental composite properties such as tensile strength, flexural strength, and storage modulus are presented.[42,45−47] However, to the best of our knowledge, mechanical properties such as Young's modulus for the neat nanotubes are not reported in the literature. In this work we have calculated the Young's moduli for single-walled halloysite nanotubes, in the same geometric optimization protocol as used for imogolite nanotubes.[31] The Young's moduli have been calculated by performing a series of relaxation calculations for different values of the cell length in the direction of the tube axis, and thus imposing either tensile or compressive strain on the nanotube. It is then possible to calculate the second derivative of the total energy with respect to the axial strain, which enables us to calculate the Young's moduli, as given by eq 3

$$Y = \frac{1}{V_o}\left(\frac{\partial^2 E}{\partial \varepsilon^2}\right)_{\varepsilon=0} \quad (3)$$

where V_o is the equilibrium volume, ε is the strain, and E is the total energy. The equilibrium volume is defined as the volume of a hollow cylindrical shell of the diameter as the nanotube, with cell length C_o. From elementary geometry, for a hollow cylinder it follows that $V_o = \pi C_o(R_{out}^2 - R_{in}^2)$, where R_{out} is the outer radius and R_{in} is the inner radius.

In Table 1, the calculated Young's moduli for *zigzag* and *armchair* single-walled nanotubes are presented, with values

in the range of 230−340 GPa. The modeled stiffness for halloysite is comparable to that of imogolite[31] (∼175−390 GPa), GaS[48] (∼270 GPa), and chrysotile nanotubes (159 ± 125 GPa).[49] The Young's moduli seem to have an asymptotic behavior with the increase of the single-walled halloysite radii. The Young's moduli of zigzag nanotubes are normally about 20−30 GPa smaller than the respective armchair nanotubes. One should mention that, according to experimental results,[49] the mechanical behavior of chrysotile nanotubes is related to the number of constituting walls in a way that Young's moduli decrease as the number of walls increase. This suggests that multiwalled nanotubes present more defects compared to single-walled ones.

Conclusions

The stability, electronic, and mechanical properties of single-walled halloysite nanotubes were studied by the density functional based tight binding method. We have investigated *zigzag* NTs with sizes (7,0)−(20,0) and *armchair* NTs with sizes (6,6)−(15,15). The optimization and the strain energies of halloysite nanotubes confirm the stability of these structures. According to our results, the strain energy of these tubes does not have a monotonic character and the most stable among them should be observed in the region of radii above 24 Å, which agrees well with experimental observations and explains the polydispersity and multiwalled character of these natural nanostructures. Besides, the strain energy is relatively insensitive to the structural details of the tubes, such as helicity.

The calculated band gap and density of states (DOS) clearly show that halloysite NTs are insulators, independent of their size. In addition, we have shown that halloysite NTs are less stiff than carbon nanotubes, but in the same magnitude order of imogolite, chrysotile, and MoS_2. The results presented herein are a contribution in an attempt to improve the knowledge about halloysite nanotubes at the molecular level. Structural, electronic, and mechanical properties are reasonably described by using single-walled halloysite nanotube models and straightforwardly extrapolated to larger models. However, it is important to note that the calculations have been performed for the anhydrous form, and the results should be considered carefully before extrapolation to the hydrous structure. Notwithstanding, further studies on multiwalled and larger diameter tubes are in progress in our laboratory.

Acknowledgment. The authors would like to thank Prof. T. Heine and Dr. A. F. Oliveira for fruitful discussion. The Brazilian agencies Fundação de Amparo à Pesquisa do Estado de Minas Gerais (FAPEMIG), Conselho Nacional para o Desenvolvimento Científico e Tecnológico (CNPq), and Coordenação de Aperfeiçoamento de Pessoal de Ensino Superior (CAPES) are gratefully acknowledged. This work has also been funded by the National Institute for Science and Technology for Mineral Resources, Water and Biodiversity, INCT-ACQUA. G.S. and A.E. also thank the ERC for support through grant INTIF No. 226639.

Supporting Information Available: Strain energy of halloysite nanotubes as a function of $1/R^2$, a comparison of halloysite and imogolite calculated strain energies and halloysite nanotubes band gap. This material is available free of charge via the Internet at http://pubs.acs.org.

References and Notes

(1) Chopra, N. G.; Luyken, R. J.; Cherrey, K.; Crespi, V. H.; Cohen, M. L.; Louie, S. G.; Zettl, A. *Science* **1995**, *269*, 966.
(2) Remskar, M. *Adv. Mater.* **2004**, *16*, 1497.
(3) Tenne, R.; Margulis, L.; Genut, M.; Hodes, G. *Nature* **1992**, *360*, 444.
(4) Lvov, Y. M.; Shchukin, D. G.; Mohwald, H.; Price, R. R. *ACS Nano* **2008**, *2*, 814.
(5) Mukherjee, S.; Bartlow, V. A.; Nair, S. *Chem. Mater.* **2005**, *17*, 4900.
(6) Pauling, L. *Proc. Natl. Acad. Sci. U.S.A.* **1930**, *16*, 578.
(7) Harris, P. J. F. *Carbon nanotubes and related structures: new materials for the 21st century*: Cambridge University Press: Cambridge, UK, 1999.
(8) Bates, T. F.; Sand, L. B.; Mink, J. F. *Science* **1950**, *111*, 512.
(9) Bates, T. F.; Hildebrand, F. A.; Swineford, A. *Am. Mineral.* **1950**, *35*, 463.
(10) Whittaker, E. J. W. *Acta Crystallogr.* **1956**, *9*, 855.
(11) Cradwick, P. D.; Wada, K.; Russell, J. D.; Yoshinag, N.; Masson, C. R.; Farmer, V. C. *Nature (London), Phys. Sci.* **1972**, *240*, 187.
(12) Joussein, E.; Petit, S.; Churchman, J.; Theng, B.; Righi, D.; Delvaux, B. *Clay Miner.* **2005**, *40*, 383.
(13) Veerabadran, N. G.; Price, R. R.; Lvov, Y. M. *Nano* **2007**, *2*, 115.
(14) Price, R. R.; Gaber, B. P. Controled release of active agents using inorganic tubules, U.S. Patent 5,651,976.
(15) Price, R. R.; Gaber, B. P.; Lvov, Y. M. *J. Microencapsulation* **2001**, *18*, 713.
(16) Shamsi, M. H.; Geckeler, K. E. *Nanotechnology* **2008**, 19.
(17) Zijian, G.; Peter, J. S.; Shik Chi, T. *Adv. Mater.* **1998**, *10*, 701.
(18) Machado, G. S.; Castro, K.; Wypych, F.; Nakagaki, S. *J. Mol. Catal. A: Chem.* **2008**, *283*, 99.
(19) Nakagaki, S.; Castro, K.; Machado, G. S.; Halma, M.; Drechsel, S. M.; Wypych, F. *J. Braz. Chem. Soc.* **2006**, *17*, 1672.
(20) Nakagaki, S.; Wypych, F. *J. Colloid Interface Sci.* **2007**, *315*, 142.
(21) Shchukin, D. G.; Zheludkevich, M.; Yasakau, K.; Lamaka, S.; Ferreira, M. G. S.; Mohwald, H. *Adv. Mater.* **2006**, *18*, 1672.
(22) Shchukin, D. G.; Mohwald, H. *Adv. Funct. Mater.* **2007**, *17*, 1451.
(23) Shchukin, D. G.; Sukhorukov, G. B.; Price, R. R.; Lvov, Y. M. *Small* **2005**, *1*, 510.
(24) Levis, S. R.; Deasy, P. B. *Int. J. Pharm.* **2003**, *253*, 145.
(25) Kelly, H. M.; Deasy, P. B.; Ziaka, E.; Claffey, N. *Int. J. Pharm.* **2004**, *274*, 167.
(26) Hedicke-Höchstötter, K.; Lim, G. T.; Altstädt, V. *Compos. Sci. Technol.* **2009**, *69*, 330.
(27) Elstner, M.; Porezag, D.; Jungnickel, G.; Elsner, J.; Haugk, M.; Frauenheim, T.; Suhai, S.; Seifert, G. *Phys. Rev. B* **1998**, *58*, 7260.
(28) Seifert, G.; Porezag, D.; Frauenheim, T. *Int. J. Quantum Chem.* **1996**, *58*, 185.
(29) Oliveira, A. F.; Seifert, G.; Heine, T.; Duarte, H. A. *J. Braz. Chem. Soc.* **2009**, *20*, 1193.
(30) Aradi, B.; Hourahine, B.; Frauenheim, T. *J. Phys. Chem. A* **2007**, *111*, 5678.
(31) Guimaraes, L.; Enyashin, A. N.; Frenzel, J.; Heine, T.; Duarte, H. A.; Seifert, G. *ACS Nano* **2007**, *1*, 362.
(32) Enyashin, A. N.; Ivanovskii, A. L. *Phys. E* **2008**, *41*, 320.
(33) Enyashin, A. N.; Ivanovskii, A. L.; Seifert, G. *Mendeleev Commun.* **2006**, 292.
(34) Monkhorst, H. J.; Pack, J. D. *Phys. Rev. B* **1976**, *13*, 5188.
(35) Neder, R. B.; Burghammer, M.; Grasl, T.; Schulz, H.; Bram, A.; Fielder, S. *Clays Clay Min.* **1999**, *47*, 487.
(36) Seifert, G.; Terrones, H.; Terrones, M.; Jungnickel, G.; Frauenheim, T. *Phys. Rev. Lett.* **2000**, *85*, 146.
(37) Enyashin, A. N.; Seifert, G. *Phys. Status Solidi B* **2005**, *242*, 1361.
(38) *International Tables For Crystallography*; Prince, E., Ed.; Kluwer Academic Publishers: Dordrecht, The Netherlands, 2004; Vol. C.
(39) Levis, S. R.; Deasy, P. B. *Int. J. Pharm.* **2002**, *243*, 125.
(40) Mitra, G. B.; Bhattacherjee, S. *Acta Crystallogr., Sect. B: Struct. Sci.* **1975**, *31*, 2851.
(41) Fu, Y. B.; Zhang, L. D. *J. Nanosci. Nanotechnol.* **2005**, *5*, 1113.
(42) Liu, M. X.; Guo, B. C.; Du, M. L.; Lei, Y. D.; Jia, D. M. *J. Polym. Sci. Res.* **2008**, *15*, 205.
(43) Theng, B. K. G.; Russell, M.; Churchman, G. J.; Parfitt, R. L. *Clays Clay Min.* **1982**, *30*, 143.
(44) Braggs, B.; Fornasiero, D.; Ralston, J.; Stsmart, R. *Clays Clay Min.* **1994**, *42*, 123.
(45) Liu, M. X.; Guo, B. C.; Du, M. L.; Cai, X. J.; Jia, D. M. *Nanotechnology* **2007**, 18.
(46) Liu, M. X.; Guo, B. C.; Lei, Y. D.; Du, M. L.; Jia, D. M. *Appl. Surf. Sci.* **2009**, *255*, 4961.
(47) Liu, M. X.; Guo, B. C.; Zou, Q. L.; Du, M. L.; Jia, D. *Nanotechnology* **2008**, 19.
(48) Kohler, T.; Frauenheim, T.; Hajnal, Z.; Seifert, G. *Phys. Rev. B* **2004**, 69.
(49) Piperno, S.; Kaplan-Ashiri, I.; Cohen, S. R.; Popovitz-Biro, R.; Wagner, H. D.; Tenne, R.; Foresti, E.; Lesci, I. G.; Roveri, N. *Adv. Funct. Mater.* **2007**, *17*, 3332.

JP100902E